# Diffractive optical elements for differential interference contrast x-ray microscopy

**Enzo Di Fabrizio, Dan Cojoc, Stefano Cabrini**

*TASC-INFM, LILIT beamline, S.S. 14 in Area Science Park , I-34012, Basovizza-Trieste, Italy*
*difabrizio@tasc.infm.it*

**Burkhard Kaulich**

*Sincrotrone Trieste, X-ray microscopy section, S.S. 14 in Area Science Park, I-34012, Basovizza-Trieste, Italy*

**Jean Susini**

*ESRF, ID21 X-ray microscopy beamline, BP 220, F-38043 Grenoble Cedex, France*

**Paolo Facci**

*INFM c/o Dept. of Physics University of Modena and Reggio Emilia, Via G. Campi 213/a, 41100 Modena, Italy*

**Thomas Wilhein**

*University for Applied Sciences, RheinAhrCampus Remagen, Suedallee 2, D-53424 Remagen, Germany*

**Abstract:** In this paper we introduce phase diffractive optical elements (DOEs) that beside simple focusing, can perform new optical functions in the range of x-rays. In particular, the intensity of the wavefront can be distributed with almost complete freedom. We calculated and fabricated high resolution DOEs that can focus a monochromatic x-ray beam into multiple spots displaced in a single or two planes along the optical axis or can shape the beam into a desired continuous geometrical pattern. The possibility to introduce a specified phase shift between the generated spots, which can increase the image contrast, is demonstrated by preliminary results obtained from computer simulations and experiments performed in visible light. The functionality of the DOEs has been tested successfully in full-field differential interference contrast (DIC) x-ray microscopy at the ID21 beamline of the European Synchrotron Radiation Facility (ESRF) operated at 4 keV photon energy.



**OCIS codes:** (180.7460) X-ray microscopy, (090.1970) Diffractive optics, (180.0180) Microscopy

## References and links

1. D. Attwood, *Soft x-rays and extreme ultraviolet radiation; principles and applications*, (Cambridge University Press, 1999)
2. G. Schneider, "Cryo X-ray microscopy with high spatial resolution in amplitude and phase contrast," Ultramicroscopy **75**, 85-104 (1998)
3. G. Schmahl, D. Rudolph, G. Schneider, P. Guttmann, B. Niemann, "Phase-contrast X-ray microscopy studies," Optik **97**, 181-182 (1994)
4. A. G. Michette, *Optical Systems for Soft X-rays*, (Plenum Press, New York, 1986)
5. E. Di Fabrizio, F. Romanato, M. Gentili, S. Cabrini, B. Kaulich, J. Susini, R. Barrertt, "High efficiency multilevel zone plates for keV X-rays," Nature **40**, 895-898 (1999)
6. G. Normarski, and A.R. Weill, "Application à la métallographie des methods interférentielles à deux ondes polarisées ," Rev. Metall. **2**, 121-128 (1955)

#2846 - $15.00 US Received August 04, 2003; Revised September 13, 2003

7. F. Zernike, "Phase contrast, a new method for the microscopic observation of transparent objects," Physica **9**, 686-698, (1942)
8. P. J. McMahon, E.D. Barone-Nugent, B.E. Allman, and K.A. Nugent, "Quantitative phase-amplitude microscopy II: differential interference contrast imaging for biological TEM," J. of Microscopy 206, 204-**208** (2002)
9. C. Preza, D.L. Snyder, J.A. Conchello, "Theoretical development and experimental evaluation of imaging models for differential-interference-contrast microscopy," J. Opt. Soc. Am. **16**, 2185-2199 (1999)
10. T. Wilhein, B. Kaulich, E. Di Fabrizio, F. Romanato, S. Cabrini, and J. Susini, "Differential interference contrast X-ray microscopy with submicron resolution," Appl. Phys. Lett. **78**, 2082-2084 (2001)
11. B. Kaulich, T. Wilhein, E. Di Fabrizio, F. Romanato, M. Altissimo, S. Cabrini, B. Fayard, and J. Susini, "Differential interference contrast X-ray microscopy with twin zone plates," J. Opt. Soc. Am A **19**, 797-806 (2002)
12. M. Bernhardt, F. Wyrowski, O. Bryngdahl, "Iterative techniques to integrate different optical functions in a diffractive phase element," Appl. Opt. **30**, 4629 (1991)
13. C. Jacobsen, M. R. Howells, "A technique for projection x-ray lithography using computer-generated holograms," J. Appl. Phys. **71**, 2993-3001 (1992)
14. A.A Firsov, A.A. Svintsov, S.I. Zaitsev, A. Erko, A, V.V. Aristov, "The first synthetic X-ray hologram: results," Opt. Commun **202**, 55-59 (2002)
15. E. Di Fabrizio, D. Cojoc, S. Cabrini, B. Kaulich, T. Wilhein, J. Susini, "Novel diffractive optics for x-ray beam shaping," SPIE Proc. **4783**, 105-114 (2002)
16. D. Cojoc, E Di Fabrizio, L. Businaro, S.Cabrini, F. Romanato, L. Vaccari, M. Altissimo, "Design and fabrication of diffractive optical elements for optical tweezer arrays by means of e-beam lithography," Microelectronic Eng. **61-62**, 963-969 (2002)
17. Applied Optics Research, "*GLAD 4.5 Theoretical Description*," 4.1-5.15 (AOR 1997)
18. J. Susini, R. Barret, B. Kaulich, S. Oestreich, and M. Salomé, "The X-ray microscopy facility at the ESRF: A status report," AIP Conf. Proc. **507**, 19-26 (2000)
19. P. Facci, D. Alliata, L. Andolfi, B. Schnyder, R. Koetz, "Formation and charcterization of protein monolayers on oxygen-exposing surfaces by multiple-step self-chemisorption," Surf. Sci. **504C**, 282-292 (2002)
20. E. Di Fabrizio, D. Cojoc, S. Cabrini, B. Kaulich, T. Wilhein, and J. Susini, "Design and fabrication of new optics for X-ray microscopy and material science," J. Phys. IV France **104**, 177-183 (2003)

## 1. Introduction

In the last decade there is an increased interest for extreme violet and x-ray microscopy. This is due to the characteristics of the beam that can be obtained in the third generation synchrotron radiation sources [1]: high brightness, low divergence and an almost monochromatic spectrum for an energy that can be tuned over a range of several keV. When a source of electromagnetic radiation is bright enough (i.e., point-like and monochromatic) new worlds open up for the designer of optical instruments and for a wider community of experimenters and theorists. This happened with the invention of the optical microscope and is still happening with x-ray microscopes of the latest generation [2,3]. Although the third generation sources have enough spatial and temporal coherence to allow the use of x-ray diffractive optics close to the diffraction limit, until now the design of new optical devices has not proceeded far beyond simple focusing optical elements. In fact, the zone plates (ZPs), which can be now considered a well established focusing element for x-rays, were invented more than hundred years ago but due to technological difficulties, have been implemented only in the last two decades [4,5].

In this paper we extend the concept of ZPs to a more general category of DOEs that can accomplish optical functions specific to DIC microscopy and general beam shaping. In particular, the intensity of the wavefront can be distributed with almost complete freedom. We describe the design and fabrication of DOEs which can divide and focus the x-ray beam into two spots displaced in the same plane or in two planes along the optical axis, or can shape the beam into a desired continuous geometrical pattern. We show also the possibility to introduce a specified phase shift between the generated spots, which can be useful to increase the image contrast, and we demonstrate it by preliminary results obtained from computer simulations and experiments performed in visible light.

#2846 - $15.00 US Received August 04, 2003; Revised September 13, 2003

## 2. Bias retardation in DIC microscopy

DIC microscopy in the Nomarski configuration is a widely used phase contrast method for the investigations of transparent specimens in visible light [6]. Such specimens, known as phase objects, cannot be seen when in focus under an ordinary transmission microscope. Phase objects retard or advance light that passes through them due to spatial variation in their refractive index and/or thickness. Phase contrast, first developed by Zernike [7] is often employed to image such objects, but the technique suffers from halo artifacts, is restricted to very thin specimen preparations, and cannot take advantage of the full condenser and objective apertures. Unlike phase contrast, DIC converts gradients in object optical path length into amplitude differences that can be visualized as improved contrast in the resulting image. The phase object is sampled by two mutually coherent waves that have a lateral displacement, $\Delta x$, called the shear and a phase displacement, $\Delta\theta$, called the bias. In visible light these two waves are obtained by illuminating the phase object with a plane polarized beam that is split by a Wollaston prism. The two waves propagate through the specimen and the microscope objective and are then recombined by another prism and an analyser into a beam of which amplitude is a function of the phase difference between them. If the shear is in the order of the object details, it is imaged into an intensity distribution that is a function of the spatial gradient of the object phase distribution. Because both beams traverse the same region of the object, DIC does not yield accurate measurements of object's refractive index or thickness. Nevertheless, it is useful to determine the orientation of phase gradients and, capitalizing on the full objective aperture, to produce thin optical sections free of obscuring disturbances from object features positioned beyond the focal plane. Moreover, a new approach was introduced recently to allow quantitative phase microscopy [8].

Under coherent illumination, the intensity distribution measured in DIC images can be written as the square modulus of the convolution of the point spread function (PSF) of the optical system and the object phase function [9]:

$$i(x,y) = \left| \iint f(x_0, y_0) h(x - x_0, y - y_0) dx_0 dy_0 \right|^2 \tag{1}$$

where $(x_0,y_0)$ and $(x,y)$ are points in the object plane and in the image plane respectively, $h(x,y)$ is the PSF and $f(x_0,y_0)=\exp(-j\Phi(x_0,y_0))$ is the phase function. If we assume an ideal PSF function for two point wavefront division with the shear $\Delta x$ in the x direction:

$$h(x,y) = 0.5\delta\left(x - \frac{\Delta x}{2}, y\right)\exp(-j\Delta\theta) + 0.5\delta\left(x + \frac{\Delta x}{2}, y\right)\exp(j\Delta\theta) \tag{2}$$

where $\delta(x,y)$ is the Dirac function, Eq. 1 becomes:

$$i(x,y) = ct\sin^2\left(\phi\left(x - \frac{\Delta x}{2}\right) - \phi\left(x + \frac{\Delta x}{2}\right) + \Delta\theta\right) \tag{3}$$

where ct is a constant that depends on the focal length of the condenser and the wavelength of the illuminating beam. If the shear $\Delta x$ is small compared to the size of the details of the object and under the assumption of a phase only transmission function for the object specimen, the phase difference in the above equation can be written as a phase gradient:

$$i(x,y) = ct\sin^2\left(\Delta x \frac{\partial\phi(x,y)}{\partial x} + \Delta\theta\right) \tag{4}$$

The intensity distribution obtained with the DIC method in the image plane is thus related to the gradient of the phase function of the object in the direction of shear. The shear $\Delta x$ and the bias $\Delta\theta$ in Eq. (4), represent in principle two useful free parameters to control the contrast of the image. Since the shear is constrained to a fixed value, the bias remains the only free parameter to play with in this regard. In order to show the influence of this parameter we

#2846 - $15.00 US Received August 04, 2003; Revised September 13, 2003

consider a one dimensional phase function that varies in a range from $-\pi$ to $\pi$ as shown in Fig. 1(a) and three PSFs with the same shear but three different bias values ($\Delta\theta= 0$, $\Delta\theta= \pi/4$ and $\Delta\theta= 3\pi/4$). The intensity distributions, obtained in the image plane, are represented in Fig. 1(b) (for clarity, the second and the third intensities are offset by –2 and –4 respectively). One can note that the spatial gradient of the phase function is pointed out in all the three cases. However, its sign (orientation) can be determined only when a bias retardation is introduced ($\Delta\theta = \pi/4$ or $3\ \pi/4$ for the 'negative' image). In addition, by using bias retardation, the image contrast is enhanced from 0.5 to 0.8. This simple example shows that beside the beam shearing, in DIC it is important to correlate the phase function of the object with a proper bias retardation. A practical consequence can be the contrast enhancement for the biological samples when the thickness is irregular. This can be realized in visible light by shifting the sliding prism along the shear direction [6]. Due to the extreme difficulties in fabricating polarizing and refractive components for the x-ray region, a different approach based on the use of a two zone plates combined into a doublet has been proposed for beam shearing [10,11] but does not allow a bias retardation control. A solution is a DOE that can incorporate the imaging function of the objective and the beam shearing and bias retardation function of the prism in the same element. X-ray DIC imaging can be thus obtained by replacing the imaging zone plate of a normal transmission x-ray microscope with the DOE having the functions mentioned above. The calculation of the phase function of the DOE is presented in the next section.

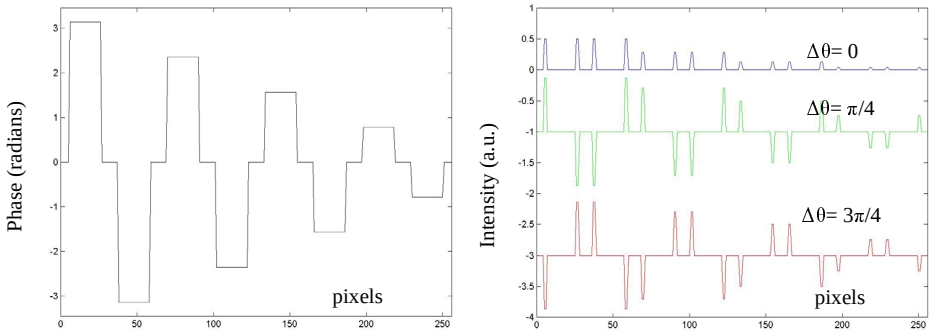


Fig. 1. (a) The phase function of a one dimensional object described in 250 pixels; (b) Intensity distributions obtained with the same shear $\Delta x = 2$ but different bias values: $\Delta\theta = 0$ - first line, $\Delta\theta = \pi/4$ - second line, and $\Delta\theta = 3\pi/4$ - third line; for clarity, the second line is offset by –2 and the third by –4

## 3. Design of DOE for beam shearing in DIC

Phase DOEs are known as optical elements that convert, by modulating only the phase, a specified illumination wave into a wave with a desired distribution of its amplitude, phase or polarization. Efficient iterative techniques, based on the thin-element approximation and the scalar diffraction theory, have been proposed to design phase DOEs with surface relief modulation for applications in visible light [12]. The extension to x-rays range was first approached in view of projection x-ray lithography [13] and the implementation of a DOE that generated a dotted pattern is reported in reference [14]. In a recent paper we also report the implementation of a DOE which generates a continuous intensity pattern [15].

A phase DOE that accomplishes beam shearing in DIC microscopy can be seen as an element that generates two spots with a specified phase difference between them. This represents a particular case of a more general DOE that, illuminated by a set of point sources, generates a set of spots arranged in a determined configuration. This type of DOEs can be calculated using a direct approach, avoiding the use of iterative algorithms. Assuming that both the light source which illuminates the DOE and the generated pattern can be described by

#2846 - $15.00 US Received August 04, 2003; Revised September 13, 2003

point sources that emit spherical waves, an estimate for the phase function is derived from the propagation and superposition of the spherical wavefronts in the plane of the DOE. Let us assume that the phase DOE is a thin element described by its transmittance function: $t(x,y)=\exp[i\Phi(x,y)]$, with the phase function $\Phi(x,y)\in [0, 2\pi]$. If $W_{in}(x,y,0)$ represents the complex amplitude of the incident wave, under the assumption of the thin element approximation, the complex amplitude of the output wave after the DOE will be:

$$W_{out}(x,y,0) = t(x,y)W_{in}(x,y,0) \tag{5}$$

where z=0 denotes the DOE's plane. For a given input-output pair of waves, satisfying the condition:

$$|W_{in}(x,y)| = |W_{out}(x,y)| \tag{6}$$

the phase function is given by:

$$\Phi(x,y)= \{\arg[W_{out}(x,y,0)] - \arg[W_{in}(x,y,0)]\}_{2\pi} \tag{7}$$

where the subscript $2\pi$ states for modulo $2\pi$. If $\{P_s(x_s,y_s,z_s), s=1,N_s\}$ is the set of $N_s$ points describing the source and $\{P_g(x_g,y_g,z_g), g=1,N_g\}$ the set of $N_g$ points describing the generated spots, the expression for the incident and output wavefronts at the point $P_e(x_e,y_e,0)$ at the DOE will be:

$$W_{in}(x_e,y_e,0) = \sum_s a_s \cos\psi_{s,e} \frac{\exp[jkr_{s,e}]}{r_{s,e}} \quad , \quad W_{out}(x_e,y_e,0) = \sum_g a_g \cos\psi_{g,e} \frac{\exp[j(kr_{g,e}+\varphi_g)]}{r_{g,e}} \tag{8}$$

where $a_{s(g)}$ are constants representing the amplitudes of the waves emitted by the point sources, $\cos\psi_{s,e} = z_s/ r_{s,e}$ is the obliquity factor, $r_{s,e}=P_sP_e$ is the distance between the source point $P_s$ and the element $P_e$ of the DOE, $r_{g,e}=P_gP_e$ is the distance between the source point $P_g$ and the element $P_e$ of the DOE, $\varphi_g$ is the initial phase of the point $P_g$ and k is the wavelength number $k=2\pi/\lambda$. Using the Eqs. (7) and (8) the phase function is calculated for the set of sampling points $\{P_e(x_e,y_e,z_e), e=1,N_e\}$ defined by a regular spaced squared grid on the DOE. The number of the sampling points $N_e$ is limited by the scalar diffraction approximation and the sampling theorem to: $D/2\lambda < N_e < D^2/\lambda z$ , where D is the lateral size of the DOE and z represents the distance from the source plane or the plane of the generated spots to the DOE. One should note that, in general, the condition (6) can not be achieved and thus the Eq. (7) gives only an estimate of the phase function. It can be optimized using global optimization methods (e.g. genetic algorithms [16]). Nevertheless, for the major part of applications this step can be avoided since the estimation is already good enough.

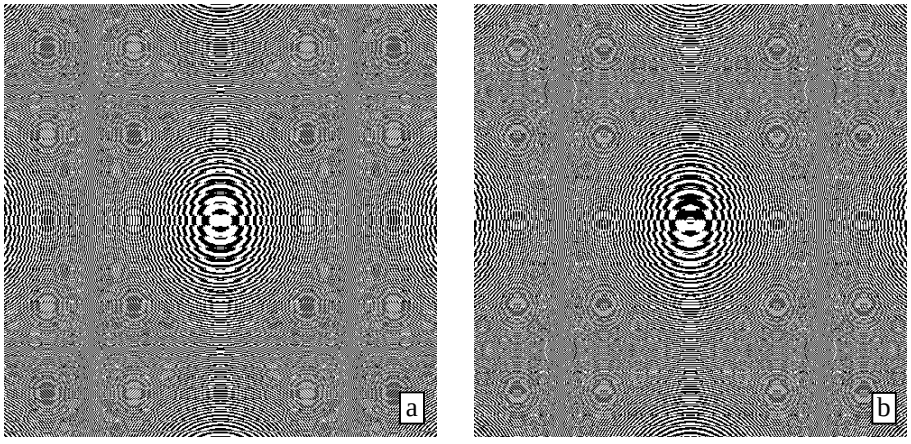


Fig. 2. DOEs producing the same beam shearing (1 mm) but different bias: a) $\Delta\theta= 0$, b) $\Delta\theta = \pi$

#2846 - $15.00 US Received August 04, 2003; Revised September 13, 2003

In order to demonstrate the validity of the method described above for beam shearing with specified bias, we calculate two DOEs that shear a plane wave into two waves focused at 1m into two spots separated by 1 mm and having the bias values $\Delta\theta = 0$ and $\Delta\theta = \pi$ respectively. Since we want to implement the DOE on the spatial light modulator (SLM) existent in the laboratory, the DOE has the following geometrical characteristics: 480x480 pixels, size 20x20 mm. The calculated binary phase DOEs are depicted in Fig. 2.

The phase distributions along the x axis in the focal plane are represented in Fig. 3 and show the presence of the desired bias retardations. They were calculated using the propagation functions of the optical software GLAD 4.7 [17], considering the wavelength of the illuminating wave $\lambda = 532$ nm. The functionality of the two DOEs has been checked experimentally by implementing them on a phase SLM (Hamamatsu PPM-X7550) and recording the intensity interference patterns that result after the focal plane on a CCD. The two patterns are represented in Fig. 4; the displacement of one pattern with half of a fringe corresponds with a phase difference of $\pi$, which is in concordance with the results obtained from simulations. Since we have chosen the geometry of the DOE tested in visible light scaling the geometry of the DOE for x-rays, we think that the same results can be expected in x-ray range.

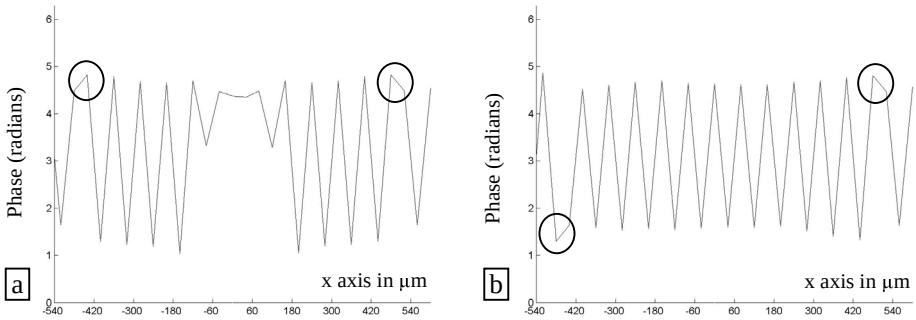


Fig 3. The phase distributions along the x axis obtained in the focal plane for the DOEs depicted in Fig. 2; (a) the phase difference between the two points pointed out by circles is $\Delta\theta = 0$ (b) the phase difference between the two points pointed out by circles is $\Delta\theta = \pi$

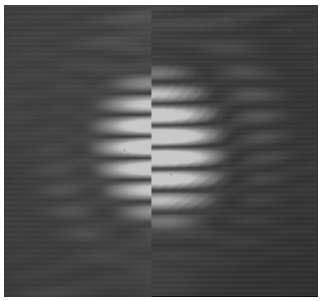

Fig.4. The experimental interference patterns obtained after the focal plane of the DOEs; the left pattern corresponding to the DOE with the bias $\Delta\theta = 0$ is shifted with half of a fringe with respect to the right pattern which corresponds to the DOE with bias retardation is $\Delta\theta = \pi$

## 4. DOE fabrication for x-ray DIC microscopy

Following the approach described in the previous section we have developed our own code to calculate phase DOEs which work in the range of x-ray wavelengths. The phase function is implemented by modulating the thickness of the gold absorber grown on a silicon nitrade membrane. The spatial variation of the thickness is given by:

#2846 - $15.00 US Received August 04, 2003; Revised September 13, 2003

$$d(x,y) = \Phi(x,y)\lambda/2\pi\delta(\lambda) \quad (9)$$

where 1-$\delta$ is the real, phase-shifting part of the refractive index. For all materials at X-ray wavelength 1-$\delta$ is very close to unity. For instance, for the gold $\delta(\lambda)\in[1.8\ 10^{-4}, 30\ 10^{-4}]$ for $\lambda\in[3, 16.31]$ Å and a $2\pi$ phase shift leads to a maximum surface profile: $d_{max}\in[544, 1667]$ nm. Considering the typical minimum lateral feature size that can be achieved by modern microfabrication techniques (t ~ 50 nm), the thin element approximation condition ($t^2 > 2\lambda d_{max}$) is satisfied and, since $t >> \lambda$, the scalar diffraction theory can be applied to the DOE design. In terms of the f-number f/D (where f is the focal length and D is the diameter of the DOE), the minimum f-number that can be obtained for a DOE working at X-ray wavelengths is in the range f/D$\in$[87, 21.2]. On the basis of the above mentioned considerations, we have fabricated two phase DOEs for a photon energy of 4 keV, whose optical functions are shown schematically in Fig. 5. They are phase binary DOEs, 0.1x0.1 mm size and the minimum structure size 100 nm, fabricated with an electron beam lithography system using a Raith ELPHY pattern generator. A 300 nm PMMA 950-K layer was spun on a 2 μm silicon nitrade covered by a thin chromium gold base plate. After the exposure and development of the resist the patterned gold absorber was grown by an electrolytic process.

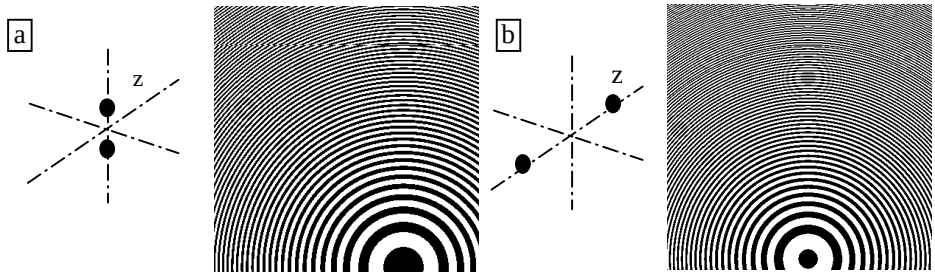


Fig. 5. Optical functions and details of two phase DOEs to generate two spots (shear $\Delta x$= 200 nm, bias $\Delta\theta$= 0) in the same focal plane at z= 50 mm from the DOE (a), and two axial spots separated by 1 mm along the optical axis at z1= 49.5 mm and z2= 50.5 mm from the DOE (b)

In Fig. 6 there are depicted two SEM images taken at different scales for the fabricated DOE that generates two spots in the same plane.

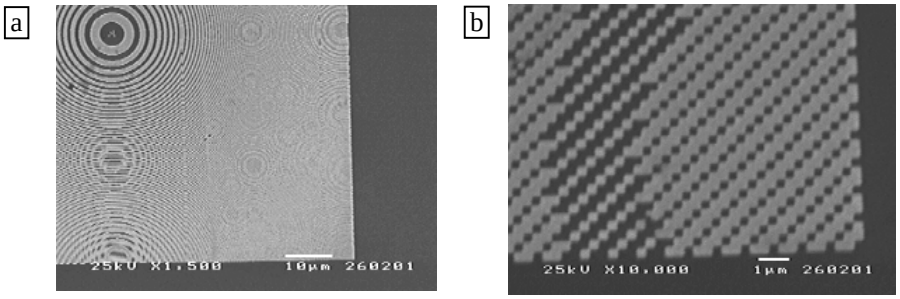


Fig. 6. SEM pictures showing an overview (a) of the DOE that generates two spots and details of the outermost area (b) whose resolution is 100 nm

## 5. DIC x-ray microscopy experiments in the full field image setup

The experiments were performed at ID21 laboratory on the full-field imaging branch line of the ESRF (European Synchrotron Radiation Facility in Grenoble), operated at 4 keV photon energy [16]. The monochromaticity of $\Delta E/E=10^{-4}$ is provided by a Si<111> double crystal monochromator. The optical scheme of the full-field imaging microscope, depicted in Fig. 7, is similar to a conventional transmission microscope with critical illumination. A condenser ZP focuses the light onto the sample and then a magnified image (150x) is obtained through the phase DOE objective onto a spatially resolving detector. The condenser used for these

#2846 - $15.00 US Received August 04, 2003; Revised September 13, 2003

experiments was an Au zone plate with a diameter of 1.2 mm, an outermost zone width of 800 nm and a focal length of 3600 mm, which has a measured first order diffraction efficiency of 19 %. The detector system consists of a fluorescent screen, converting the x-ray photons into visible light, and microscope optics, which projects the 3x magnified image onto a CCD camera (with 1340x1300 pixels and a pixel size of 20 x 20 $\mu m^2$). Measured flux in the condenser probe of 60 x 20 $\mu m^2$ is $5x10^7$ ph/s/Si<111>bandwidth. The DOE optics with a focal length of 50 mm at 4 keV were used as objective lenses. The small numerical aperture of the condenser illumination ($3x10^{-4}$) made it necessary to add an additional aperture in the optical scheme (not represented in Fig. 7). In the case of image formation with low numerical aperture, the focal area of the –1 order of the DOE is close to the specimen plane. Thus, it generates a shadow projection, which overlaps the +1 order. Therefore, a 20 µm diameter pinhole is aligned slightly off-axis and close to the specimen plane in order to separate the –1 order projection and the +1 order image.

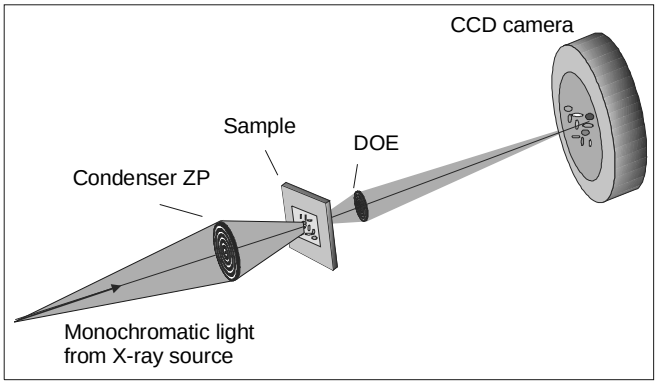


Fig. 7. Optical setup of the full-field imaging microscope

In order to show the usefulness of the phase DOEs in DIC imaging we have chosen two test patterns having square and ring shapes made by PMMA, 1.5 micron thick. The images depicted in Fig. 8(a) and Fig. 8(d) were obtained using a standard ZP as objective and reveal a very low contrast since the sample transparency is about 99 % at 4 keV. The images depicted in Fig. 8(b) and Fig. 8(e) were obtained replacing the ZP with the phase DOE of which optical function is depicted in Fig. 5(a). Beside the high contrast, the images reveal the spatial gradient of the object phase function as predicted by the theoretical consideration presented in the first section (i.e. the gradient along the direction of shear is pointed out but its orientation not).

#2846 - $15.00 US Received August 04, 2003; Revised September 13, 2003

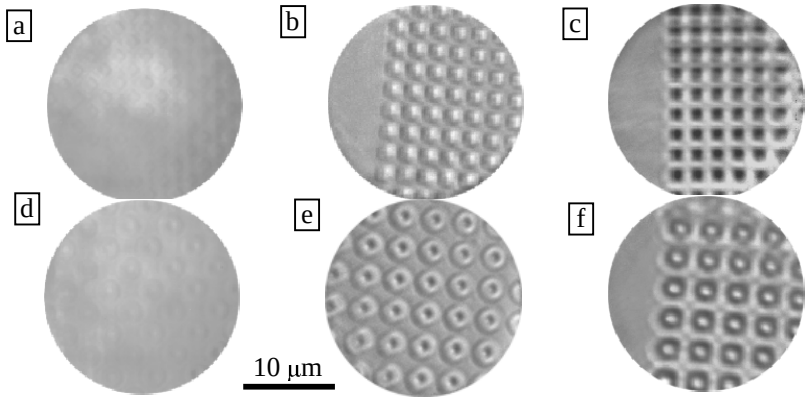


Fig. 8. Images obtained for PMMA square shaped and ring shaped test patterns obtained in transmission x-ray microscopy by using standard ZP - (a),(d) and phase DOEs for DIC - (b), (c), (e), and (f) (see the text for the description of the images).

The images depicted in Fig. 8(c) and Fig. 8(f) were obtained using the phase DOE that generates two axial spots, as shown in Fig. 5(b). One can observe that these high contrast images reveal also a bright to dark conversion of the grey levels. In this case the PSF depends on the radial coordinate r, and the shear $\Delta x$ becomes the radial shear $\Delta r$, which is related to the two wavefronts generated by the DOE; the bias retardation $\Delta\theta$ is zero. The intensity distribution in the DIC image can be derived from Eq. (1) introducing the proper PSF and consequently obtaining an additional constant term and a linear sinusoidal term in Eq. 4. The last term contributes to the bright to dark conversion observed in the images. A more detailed theoretical analysis will be given in a further work. Since its circular symmetry this DOE allows to obtain a better image for the ring shaped pattern than for the square one and make us think that the image formation, when continuous beam-shaped intensity distribution is generated in the sample plane, is influenced by the symmetry of both pattern and light distribution. In other words, patterns with the same symmetry of the light distribution are well "recognised" in phase contrast microscopy.

In order to apply the previous ideas to biological samples, we used the two coaxial spot DOE to image a monolayer of yeast cells. In this case the circular symmetry of the DOE enhances the imaging of an array of cells. Moreover, due to the particular light distribution, the depth of focus is increased. This reduces cell damage during the time necessary to find the optimal focal plane. The samples of Saccharomyces Cerevisiae have been prepared by exposing the surface of the membrane to a water solution of 2-mercaptoethylamine which binds as a self assembled monolayer to the gold film present onto the silicon nitrade support. Thereafter, incubation with glutharic dialdehyde gave rise to an adhesive surface suitable for immobilising yeast cells (as well as any other cell or protein [19]) by binding the surface amines present on the cell wall. The membrane was then incubated with a buffer suspension of Saccharomyces (50.000 cells/ml) for 45 min and then rinsed in tris HCl 10 mM pH 7.6 buffer to get rid of physisorbed cells or debris. The samples were eventually dried in a $N_2$ flow prior to use. Samples prepared by this method showed extended cellular patches, which were stable for several days even in ambient conditions. In this case the circular symmetry of the DOE enhances the imaging of an array of cells. Moreover, due to the particular light distribution, the depth of focus is increased. This reduces cell damage during the time necessary to find the optimal focal plane. Fig. 9 shows in shades of brown the result of transmission scanning imaging of the cell aggregate. We accomplished the same imaging experiment with a single zone plate and, due to the low contrast, no detectable image was obtained. This is due to the low absorption coefficient of the cell at 4 keV (in fact its transmission can be estimated to be higher than 99 %).

#2846 - $15.00 US Received August 04, 2003; Revised September 13, 2003

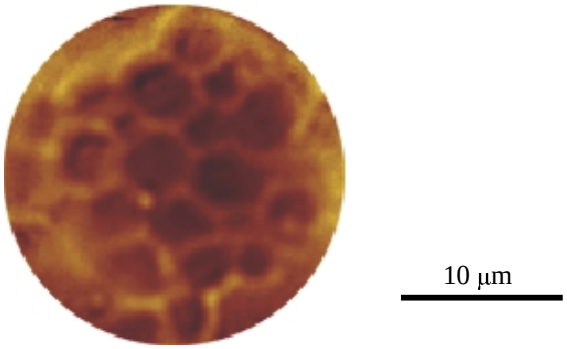


Fig. 9. Imaging of an array of yeast cells in full field DIC with a two axial spot phase DOE as objective

In order to fully test the design and fabrication capabilities, we fabricated also a phase DOE that shapes the x-ray beam into a continuous profile without any particular symmetry (the logo OK !). To image the logo on the CCD we modified the standard setup of the transmission microscope: the phase DOE replaced the condenser ZP and a standard ZP was used as objective lens. In Fig. 10 is shown the measured intensity distribution having the logo OK! shape. The picture is clearly visible and the details are on the scale of 200 nm, as expected by the design.

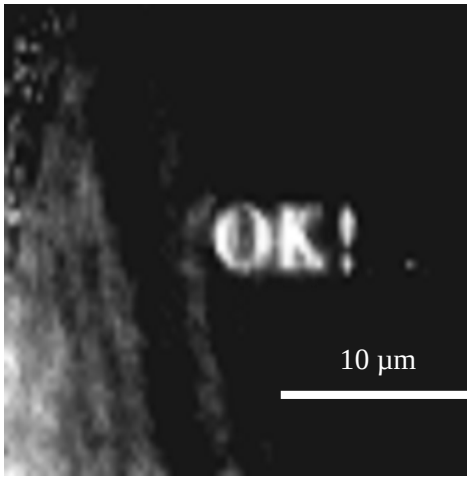


Fig. 10. X-ray beam shaping: magnified logo OK! image on CCD the detector

## 6. Conclusions

We present the design and fabrication of new phase DOEs to accomplish new optical functions in the field of DIC x-ray microscopy. Beside this application, this approach can be applied to obtain DOEs which can accomplish a variety of applications in x-ray beam shaping, bio-imaging and nanofabrication. Future trends in the biophysical applications of this technique can take advantage of the possibility of measuring simultaneously both topography and fluorescence. We already applied the DIC imaging combined with x-ray fluorescence, in a scanning configuration, to a $SiO_2$ fiber air pollution filter [20]. Future work will be directed to study the uptake and localisation of heavy metals with various cells. The two combined imaging methods should enable us to locate the metal with sub-cellular resolution, thus answering still open questions on the mechanisms governing this phenomenon.

#2846 - $15.00 US Received August 04, 2003; Revised September 13, 2003

The general beam shaping experiment was conceived in view of lithographic and material science applications. In fact, the freedom in redistributing the electromagnetic field in the focal plane suggests a maskless way to transfer the information onto a substrate. The sensitive material on the surface can be a resist or a precursor gas, in the case of CVD, whose interaction with the surface can be induced by photons. These maskless and resistless processes offer some advantage respect to the conventional lithography because the patterning can be done directly without the use of resist (in the case of CVD) and without a lithographic mask in the case of beam shaping. Moreover, these techniques can reach resolution of a few nanometers. In the case of x-ray lithography with conventional resists, the beam shaping can be advantageous both in full beam shaping and in multi-spot DOE. Combining the optical functions with an automatic shuttering device it would be possible to print simultaneously pre-defined geometrical structures and directly "write" with multi-spot optics a specific pattern. The depth of focus of this kind of optics is in the range of few microns. For high resolution lithographic fabrication this does not represent a limitation because the aspect ratio is high. Instead, it is a limitation for deep lithography applications.

**Acknowledgement**

The authors would like to thank gratefully the Dr.s M. Salome', B. Fayard, O. Dhez, U. Neuhausler and R. Baker for their outstanding support during the measurements at ESRF ID21 beamline.

#2846 - $15.00 US Received August 04, 2003; Revised September 13, 2003